Synoptic weather patterns associated with heavy La Niña rainfall in the southwest United States

N. Feldl,[1] and G. H. Roe,[2]

N. Feldl, Department of Atmospheric Sciences, University of Washington, 408 ATG Building, Seattle, WA 98195-1640, USA. (feldl@u.washington.edu)

G. H. Roe, Department of Earth and Space Sciences, University of Washington, 070 Johnson Hall, Seattle, WA 98195-1310, USA.

[1]Department of Atmospheric Sciences,
University of Washington, Seattle,
Washington, USA.

[2]Department of Earth and Space Sciences,
University of Washington, Seattle,
Washington, USA.

La Niña winters exhibit significant local enhancement of heavy rainfall in the southwest United States, relative to El Niño. This contrasts with average daily rainfall intensity, which is instead increased during El Niño. The present study explores the relationship between heavy rainfall and associated atmospheric circulation patterns. Using composite analysis, we find that heavy rainfall events in the southwest arise from the presence of a persistent offshore trough and simultaneous emplacement of a strong source of subtropical water vapor. Greater intensity of these storms during La Niña is consistent with a deeper offshore trough leading to strengthened moisture fluxes. Composite circulation patterns survive amongst a large degree of synoptic variability, highlighting the importance of understanding this variability when making regional climate predictions.

1. Introduction

Understanding controls on heavy rainfall is a principle goal of climate impacts research, and for assessing natural hazard risk. One particular challenge centers on how such rainfall events respond to variability in large-scale atmospheric circulation. A wide range of space and time scales must be tackled. The frequency, intensity, and spatial extent of rainfall all vary, and large-scale circulation depends on distant forcing. For instance, changes in tropical Pacific Ocean heating and convection comprising El Niño Southern Oscillation (ENSO) are associated with far-reaching temperature and rainfall anomalies [*Trenberth et al.*, 1998, and references therein]. Linking climate variability and associated regional weather impacts is of great public interest in affected regions (such as the southwest United States in the case of ENSO), and is particularly relevant to societal issues such as flood and landslide mitigation and reservoir management.

Using ENSO as a case study of changes in midlatitude atmospheric circulation patterns, *Feldl and Roe* [2010] (hereafter, FR10) find that, consistent with conventional wisdom, wintertime mean daily rainfall intensity is larger during El Niño relative to La Niña in the southwest (vice versa in the northwest). However, contrary to expectations, FR10 also demonstrate that extreme southwest rainfall is locally enhanced during La Niña, and this result is significant in the regional average. In the present study we seek to understand the causes by exploring synoptic conditions associated with heavy ENSO rainfall in the American West.

We consider daily rainfall over the southwest (SW) United States defined by 40-49.5°N, 116-126.25°W. Fig. 1 reproduces the findings of FR10 but for a narrowed coastal re-

gion. This region exhibits strikingly coherent spatial rainfall patterns in the mean ENSO response; in particular, the northern boundary coincides with the northern extent of increases in mean daily rainfall intensity during El Niño. In addition to considering the full range of daily rainfall rates, we apply statistical tests to evaluate the regional mean of aggregate rainfall exceeding a given daily threshold. In the northwest (NW), for all thresholds considered, heavy rainfall conforms to the expected picture of increases during La Niña relative to El Niño. However in the SW (Fig. 1a), La Niña rainfall overtakes El Niño as the threshold is raised. For thresholds exceeding 18 mm/day, La Niña actually exhibits a statistically significant increase in mean daily rainfall intensity in the SW, relative to El Niño.

Fig. 1b shows that diffuse increases in heavy La Niña rainfall over El Niño are apparent across the SW, although to a lesser degree in southernmost California. Much of the spatial structure of rainfall differences is likely determined by the relationship between mean wind direction and mountain range orientation, with flow perpendicular to the range leading to lifting along the windward flank and orographic rainfall. We emphasize this is an intensity rather than frequency signal, and El Niño winters do indeed experience more frequent heavy SW rainfall, for all thresholds [FR10]. Reconciling changes in frequency and intensity requires a redistribution of the fraction of aggregate rainfall events per threshold, with La Niña receiving a larger proportion of its total rainy days from extreme rainfall, compared to El Niño.

2. Data and Methods

We seek to understand prevailing synoptic conditions during locally heavy wintertime (November through March) El Niño and La Niña rainfall. Three datasets are used:

1. Rainfall is obtained from CPC Unified Rain Gauge Database of gridded (0.25° x 0.25°) daily station data for 1948-1998 [*Higgins et al.*, 2000b]. Rainfall rates represent an average over each grid cell.

2. Strong ENSO events are selected based on the wintertime SST anomaly within the Niño 3.4 region (5°N-5°S, 170-120°W) [*Trenberth*, 1997] exceeding ±1K. While much of the literature refers to warm and cold ENSO events, we retain El Niño and La Niña nomenclature.

3. Daily synoptic fields other than rainfall are from NCEP/NCAR Reanalysis [*Kalnay et al.*, 1996] for the same period as the rainfall.

We index all La Niña and El Niño days which record heavy rainfall (defined as $\geq$20 mm/day) in the SW (for at least one grid cell). For La Niña, 384 days fit this criteria, or 34% of the total number of La Niña days in our 50-year window, and for El Niño, 526 days (43%). In Section 3.1 we present composites of synoptic state for heavy El Niño and La Niña rainfall in the SW. All figures show unweighted composites, or in other words, composites in which each day is weighted equally. In Section 3.2 we discuss variability amongst composite members. Results are summarized in Section 4.

3. Results

3.1. Composite Analysis

Figs. 2a-b show mean daily 500 hPa geopotential height and relative vorticity for El Niño and La Niña storms. The relative vorticity reflects local flow curvature and highlights the position of the offshore trough. This mean circulation demonstrates characteristic ENSO features. For instance, observed ridging of 500 hPa heights over the Rockies and associated split flow is typical of El Niño conditions [*DeWeaver and Nigam*, 2002]. Likewise, an eastward extension and poleward shift of the La Niña jet is apparent from the shift of the Pacific vorticity couplet (Fig. 2b).

Moreover, we note that relative vorticity during La Niña storms (Fig. 2b) is enhanced compared to El Niño (Fig. 2a), suggestive of a deeper trough. SW rainfall is too distant to be attributed directly to large-scale vorticity advection. Rather other factors, such as frontal processes, must contribute. Interestingly, there is a hint of a zone of enhanced relative vorticity persisting across the southern U.S. during El Niño storms. This is consistent with a westward extension of the downstream trough, and may be related to far-south increases in heavy El Niño rainfall (Fig. 1b).

Figs. 2c-d show composite 500 hPa geopotential height anomalies for heavy La Niña and El Niño rainfall. The anomalies are calculated by subtracting the 30-day running mean, which removes seasonal changes in background state that occur over the five-month winter. We see that, for both El Niño and La Niña, heavy SW rainfall is associated with a large offshore trough. These anomalies are statistically different from the mean field according to the t test at the 5% significance level (allowing for a 5% chance of identifying an anomaly where none exists). During La Niña the maximum anomaly is displaced northwards, but

is deeper (17 m on average) and so it also extends farther south. This deep offshore trough during La Niña storms in the SW is consistent with the enhanced vorticity field (Fig. 2b).

The 500 hPa trough is particularly persistent during heavy La Niña rainfall in the SW. We perform lagged composite analyses to evaluate persistence (not shown), and find that the anomaly survives for several days before and after heavy rainfall events. For instance, the e-folding timescale indicates the anomaly on average persists for 5 days after heavy rainfall. In comparison, the e-folding decay time of an average 500 hPa anomaly (on all days) is only 3.4 days for a sample winter. Both of these decay times were calculated at the location of the composite trough maximum.

Some insights into differences between El Niño and La Niña rainfall are apparent from composites of atmospheric moisture content and advection. Fig. 3 shows column-integrated water vapor and 850 hPa wind for heavy rainy days (left) and all precipitating days (right) in the SW. Overall, heavy rainfall during both El Niño and La Niña is associated with enhanced offshore moisture, compared to all precipitating days. However the subtropical moisture reservoir is also slightly enhanced (in both area and magnitude) during heavy La Niña rainfall relative to El Niño. In addition, 500-1000 hPa geopotential thickness (not shown) indicates a warmer lower troposphere during La Niña storms and thus a higher moisture-carrying capacity.

Fig. 3 also shows spatial variability in the strength and direction of mean column-integrated moisture flux into the SW (see compass plots). The black arrow in the compass plots represents moisture flux averaged over a SW coastal subregion. Focusing on heavy rainfall, on average we see a more southwesterly moisture flux during El Niño,

consistent with general ENSO conditions (247° compared to 267° during La Niña), and strengthened moisture fluxes during La Niña relative to El Niño (127 kg(ms)$^{-1}$ compared to 110 kg(ms)$^{-1}$). In both cases the moisture fluxes are considerably larger than the climatological average or the ENSO average when the full range of rainfall is retained.

From Fig. 3 the role of orographic enhancement on local rainfall patterns becomes apparent. Regions associated with flow impinging on the windward flank of mountain ranges during La Niña (e.g. Sierra Nevada) show increased heavy La Niña rainfall (c.f. Fig. 1b). Whereas mountain ranges instead oriented perpendicular to the more southwesterly El Niño winds (e.g. Transverse Ranges of Southern California) demonstrate increased heavy El Niño rainfall. Thus a combination of large-scale weather patterns and local effects determines the ENSO rainfall response.

In summary of the compositing, heavy SW rainfall events arise from the presence of a persistent offshore trough and simultaneous emplacement of a strong source of subtropical water vapor. Greater intensity of these storms during La Niña is consistent with a deeper offshore trough leading to enhanced (and more westerly) moisture flux. This mechanism is comparable to the one proposed by *Higgins et al.* [2000a] to explain extreme rainfall events in the western U.S. during neutral years preceding El Niño. However overall similarities in moisture content for Figs. 3a and 3c suggest mean flow differences may in fact be of greater importance than moisture differences for heavy rainfall.

3.2. Variability

Observed superposition of moisture and circulation anomalies shows some similarity to classic Pineapple Express events, a synoptic description of intensely-precipitating storms

that impinge on the West Coast, originating as warm and wet air masses transported from the tropics near Hawaii [*Dettinger*, 2004]. However the well-defined and, in particular, narrow plume of moisture which characterizes an atmospheric river is absent from our composite. Are atmospheric rivers simply washed out in the average? The record-breaking 1955 Christmas Eve storm which led to flooding in Yuba City, California, [*Cole and Scanlon*, 1955] was concurrent with an offshore plume of tropically-sourced water vapor with column-integrated moisture values exceeding 40 kg m^{-2}. In fact, December of 1995 remains ranked as the wettest month on record for this region (according to the California Department of Water Resources northern Sierra Nevada eight-station index, available at http://www.cnrfc.noaa.gov/) with 30.83 inches of rainfall. This case is dramatic, but also leads one to wonder what fraction of daily composite members display distinctive Pineapple Express characteristics.

We emphasize that composite members display a large degree of variability in circulation patterns comprising the mean. Fig. 4 shows illustrative sample members of the La Niña storm composite, for column-integrated moisture and 500 hPa geopotential height. Deep troughs are prevalent (e.g. Fig. 4a) and often lead to cut-off lows (e.g. Fig. 4d), during La Niña storms in the SW. These patterns are reflected in composite 500 hPa geopotential height anomalies (Fig. 2d). In contrast, during heavy El Niño rainfall, troughs tend to dig less deep, and we see more general southwesterly flow upstream of the SW (not shown).

Focusing on column-integrated moisture, individual days comprising the composite exhibit a wide range of scenarios. The most common case is of moderate ($\sim$25 kg m^{-2}) moisture emplacement on the leading trough edge (e.g. Fig. 4a). Only a fraction of heavy

La Niña rainfall events (no more than 20-25%) can be characterized as Pineapple Express-like storms (e.g. Fig. 4c), whereas on other days the relationship between rainfall and synoptic conditions is more nuanced. Strong rainfall events also occur in the case of an offshore ridge (e.g. Fig. 4b) and westerly flow (e.g. Fig. 4e), and even during general lack of widespread available moisture (e.g. Fig. 4f). In considering the relationship between weather and climate, we note the large degree of variability exhibited in daily fields, and that the composite is a residual of this variability.

Inspection of daily rainfall maps for rates exceeding 20 mm/day shows that the largest La Niña storms tend to sweep across the entire western United States. This implicates trailing cold fronts in explaining heavy La Niña rainfall south of 40°N. Since cold fronts and associated rainfall tend to stretch along the trough axis, we expect concurrent (or leading by a day) heavy rainfall in the NW (as for ∼88% of our heavy SW events). Moreover heavy SW rainfall is likely to be more heavy during La Niña due to increased tropospheric temperature and moisture, relative to the NW and to El Niño, as stated earlier. Sometimes La Niña storms do hit the SW coast only, with no associated heavy NW rainfall. And occasionally we see isolated grid cells of heavy rainfall, consistent with embedded frontal convective elements and perhaps concurrent with widespread drizzle.

4. Summary

The goal of this analysis was to explore synoptic conditions behind an unusual and significant rainfall signal. We analyze atmospheric circulation patterns producing enhancement of heavy La Niña rainfall in the southwest United States (even though the frequency of heavy rainfall is actually increased during El Niño). Composite analyses

show that heavy La Niña rainfall is consistent with a persistent and deep offshore trough that taps into enhanced tropospheric moisture and advects it to the SW. We emphasize the large amount of interstorm variability, with only a fraction of events fitting canonical Pineapple Express conditions. This behavior highlights the importance of understanding natural variability when making predictions of important atmospheric phenomena such as extreme rainfall. Depending on the impact of interest, be it frequency and spatial extent of heavy rainfall, or intensity of local rainfall, either El Niño or La Niña conditions may have the strongest effect.

Acknowledgments. We thank Lynn McMurdie, Chris Bretherton, and Greg Hakim for insightful conversations. This work was supported by the National Science Foundation (EAR-0642835).

References

Bretherton, C. S., M. Widmann, V. P. Dymnikov, J. M. Wallace, and I. Bladé, The Effective Number of Spatial Degrees of Freedom of a Time-Varying Field, *Journal of Climate*, *12*, 1990–2009, 1999.

Cole, R. O., and J. P. Scanlon, Flood-producing rains in northern and central California, december 16-26, 1955, *Monthly Weather Review*, *December 1955*, 336–347, 1955.

Dettinger, M., Fifty-Two Years of 'Pineapple-Express' Storms across the West Coast of North America, *Tech. Rep. CEC-5000-2005-004*, U. S. Geological Survey, Scripps Institution of Oceanography for the California Energy Commission, PIER Energy-Related Environmental Research, 2004.

DeWeaver, E., and S. Nigam, Linearity in ENSO's Atmospheric Response, *Journal of Climate*, *15*, 2446–2461, 2002.

Feldl, N., and G. H. Roe, Climate variability and the shape of daily precipitation: A case study of ENSO and the American West, *Journal of Climate*, in review, 2010.

Higgins, R. W., J.-K. E. Schemm, W. Shi, and A. Leetmaa, Extreme Precipitation Events in the Western United States Related to Tropical Forcing, *Journal of Climate*, *13*, 793–820, 2000a.

Higgins, R. W., W. Shi, E. Yarosh, and R. Joyce, Improved United States precipitation quality control system and analysis, NCEP/Climate Prediction Center ATLAS No. 7, *Tech. rep.*, National Oceanic and Atmospheric Administration, 2000b.

Kalnay, E., et al., The NCEP/NCAR Reanalysis 40-year Project, *Bulletin of the American Meteorological Society*, *77*, 437–472, 1996.

Trenberth, K. E., The Definition of El Niño, *Bulletin of the American Meteorological Society*, *78*, 2771–2777, 1997.

Trenberth, K. E., G. W. Branstator, D. Karoly, A. Kumar, N.-C. Lau, and C. Ropelewski, Progress during TOGA in understanding and modeling global teleconnections associated with tropical sea surface temperature, *Journal of Geophysical Research*, *103*(C7), 14,291–14,324, 1998.

von Storch, H., and F. W. Zwiers, *Statistical Analysis in Climate Research*, 484 pp., Cambridge University Press, Cambridge, United Kingdom and New York, NY, USA, 1999.

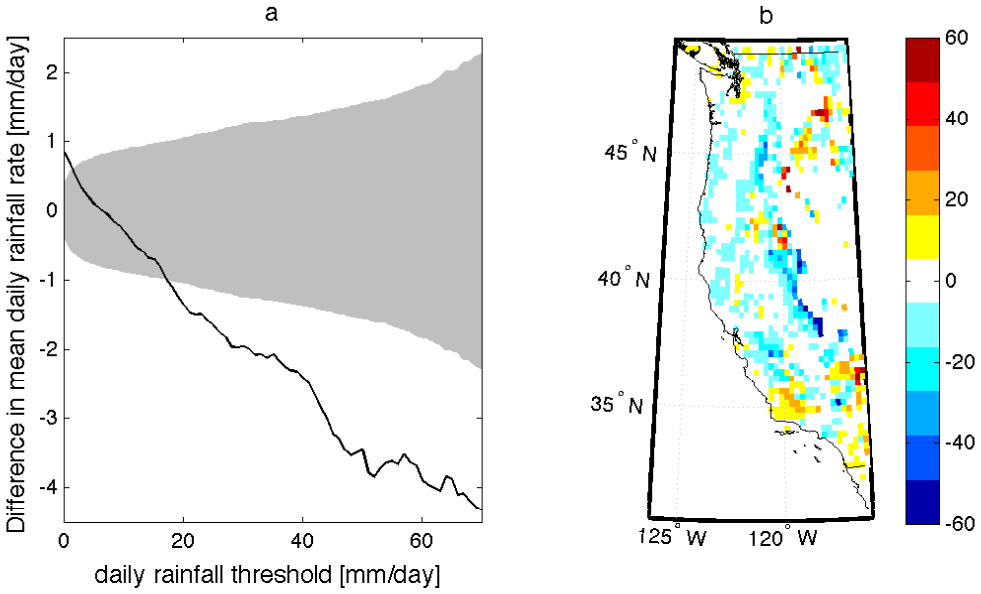

Figure 1. (*a*) Wintertime mean daily aggregate rainfall rate for El Niño minus La Niña as a function of threshold in the SW. Gray envelope indicates 95% confidence limits for the two-sample t test, after correcting for spatial and temporal correlation of rainfall data [*Bretherton et al.*, 1999; *von Storch and Zwiers*, 1999]. (*b*) Spatial patterns of percent differences in mean daily rainfall intensity (El Niño minus La Niña) for events ≥20 mm/day. Modified from FR10.

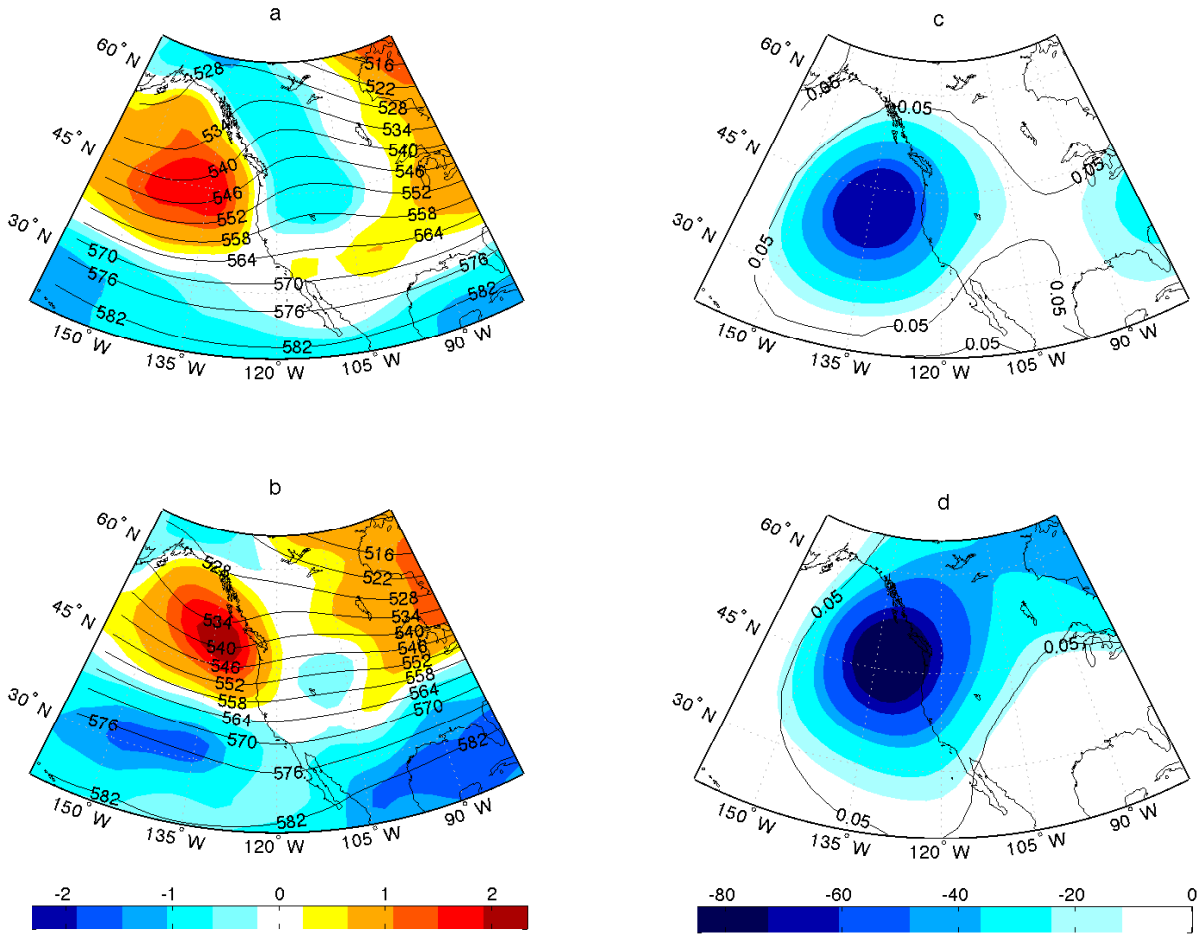

Figure 2. *Left* Composite 500 hPa relative vorticity [10^{-5} s^{-1}] (shaded) and mean geopotential height [dam] (contours) for heavy SW rainfall. The top panel shows El Niño, the bottom panel, La Niña. *Right* Composite 500 hPa geopotential height anomalies [m] from the 30-day running mean, also for heavy SW rainfall. 95% confidence limits according to the t test are indicated by the solid contour. Heavy rainfall events are defined as $\geq$20 mm/day.

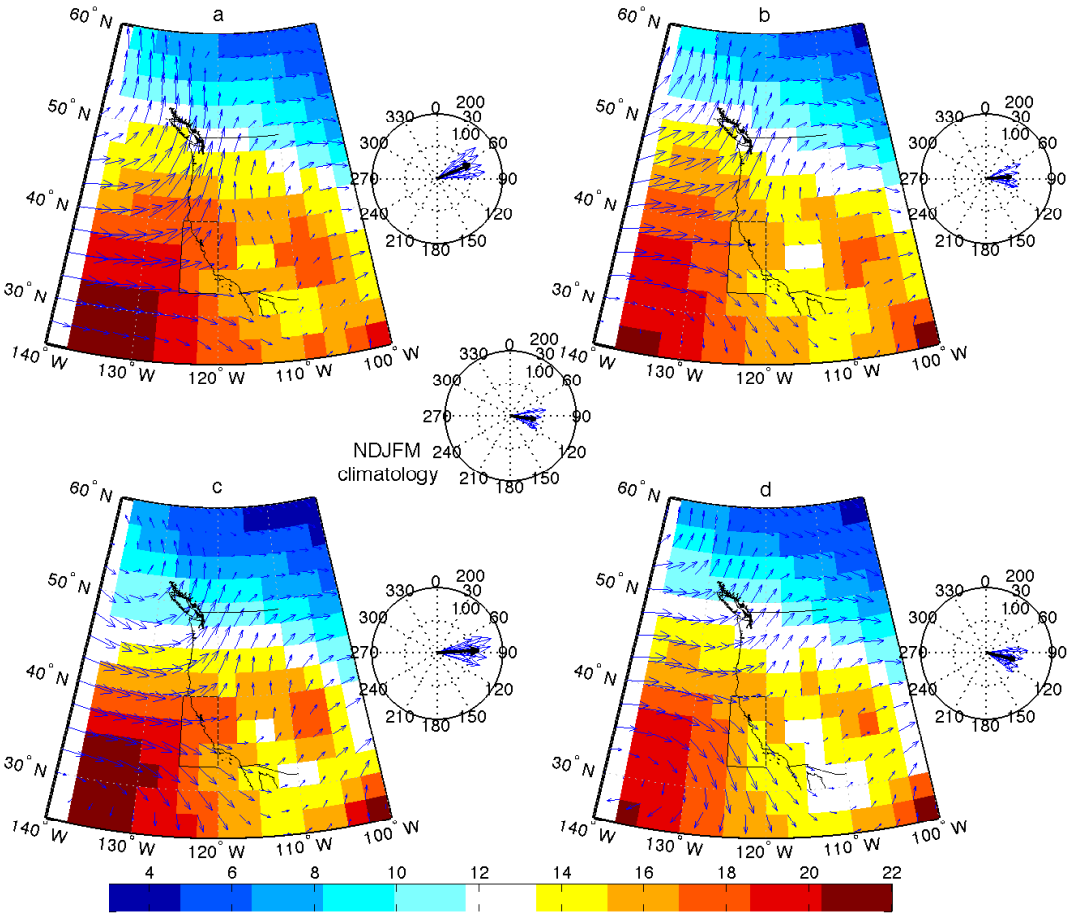

Figure 3. Composite column-integrated moisture [kg m^{-2}] (shaded) and 850 mb winds (vectors) for (*left*) heavy rainfall (≥20 mm/day) and (*right*) all precipitating days, in the SW. The top panel shows El Niño, the bottom panel, La Niña. Insets show mean column-integrated moisture flux [kg $(ms)^{-1}$] for boxed region, with the grand mean indicated by the black vector. The center compass plot indicates winter climatological values of column-integrated moisture flux for boxed region.

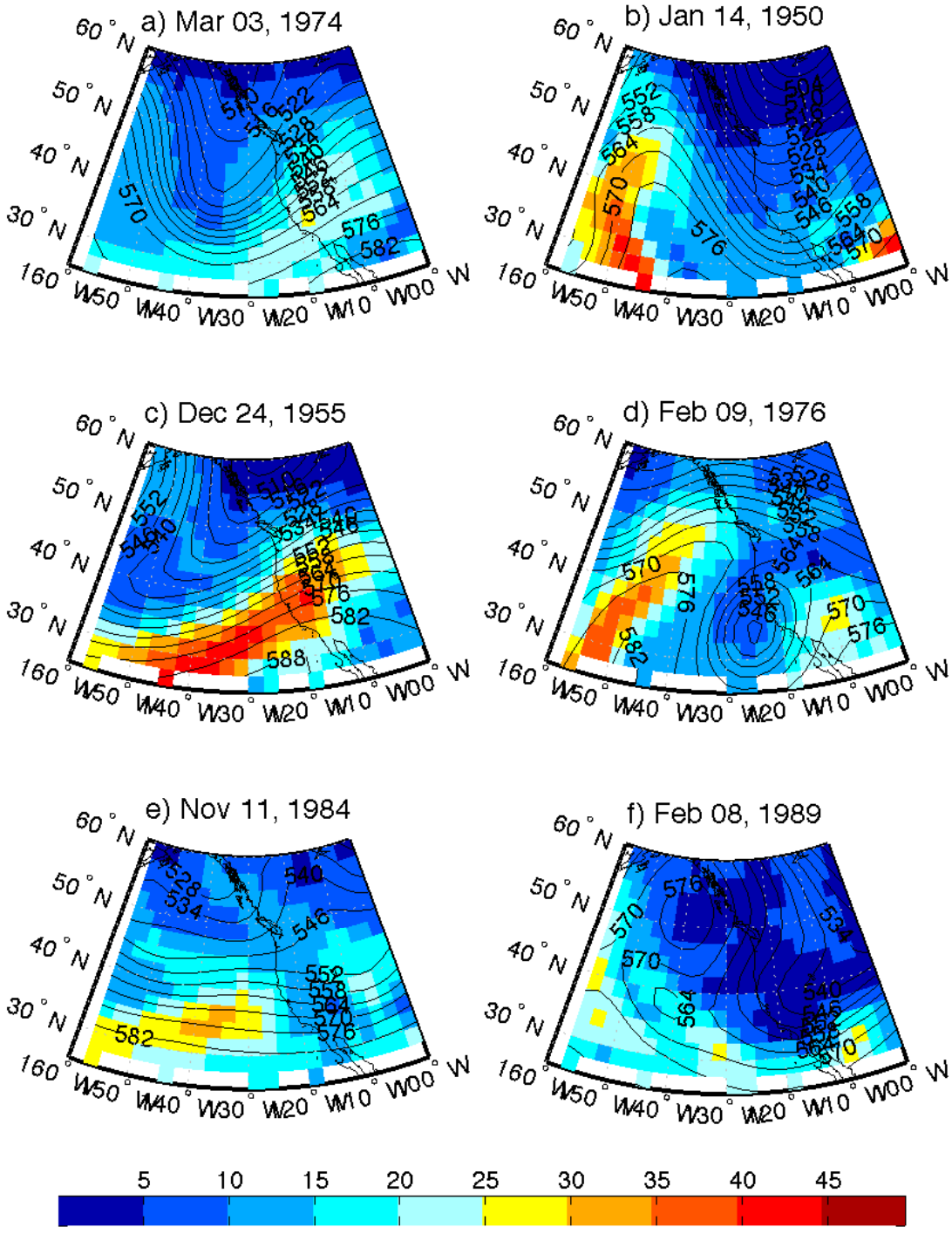

Figure 4. Composite members of column-integrated (1000-300 hPa) moisture [kg m^{-2}] (shaded) and 500 hPa geopotential heights [dam] (contours) for heavy (≥20 mm/day) La Niña rainfall in the SW. By visual inspection of daily fields, no more than 20-25% of these events display characteristic Pineapple Express features.